Various Cross-Range Resolution Techniques Applied to an Eight-Channel 77 GHz Sensor

Peter Feil #1, Winfried Mayer #2, Wolfgang Menzel #3

#Institute of Microwave Techniques, University of Ulm
Albert-Einstein-Allee 41, 89069 Ulm, Germany
1 Peter.Feil@uni-ulm.de
2 Winfried.Mayer@ieee.org
3 Wolfgang.Menzel@uni-ulm.de

***Abstract*— Different radar imaging algorithms have been developed and applied to an experimental 77 GHz eight-channel FMCW (Frequency Modulated Continuous Wave) sensor. The sensor uses a single TX antenna and an eight beam RX antenna. The RX antenna provides different beamwidths by the use of dielectric radiators as feeds. Both antennas are realised as planar folded reflectarrays.**

I. Sensor Overview

Future automotive radar sensors are intended to integrate different medium and long range functionalities in one single system (e.g. autonomous cruise control (ACC) and obstacle detection in stop and go situations). This requires a wide cross-range coverage, which can be obtained by multi-channel sensors and appropriate antenna characteristics [1]. The principal sensor setup and a photograph of the sensor are shown in Fig. 1. The 77 GHz FMCW-module used for waveform synthesis and coherent demodulation is an improved version of the module presented in [2]. In this module all active and passive mm-wave components are integrated with their supporting electronics in one RF multilayer PCB. It is stacked together with three additional PCBs containing IF processing, power supply, and control electronics. A rectangular waveguide manifold forms the connection between the radar module and the TX antenna and the eight beam RX antenna.

II. Antennas

Both antennas are folded planar reflectarrays as presented in [3] and [4]. They have a circular cross-section with diameters 110 mm (TX) and 133 mm (RX). The TX antenna provides a sector characteristic and covers an azimuthal range of $\pm 30°$ with a half-power beamwidth of $4°$ in elevation. The RX antenna is a modified multi-beam antenna according to [4]. The beamwidths of the antenna of a combined medium and long range automotive sensor shall be narrow in the boresight direction. The outer beams have to be wider in azimuthal direction to provide an extended cross-range coverage at medium ranges. To fulfil these requirements using only a single aperture waveguide excited dielectric elements are used as feeds (cf. Fig. 2). These feed elements are designed to focus the power in the azimuthal plane and in consequence broaden the beamwidth of the reflector in this plane.

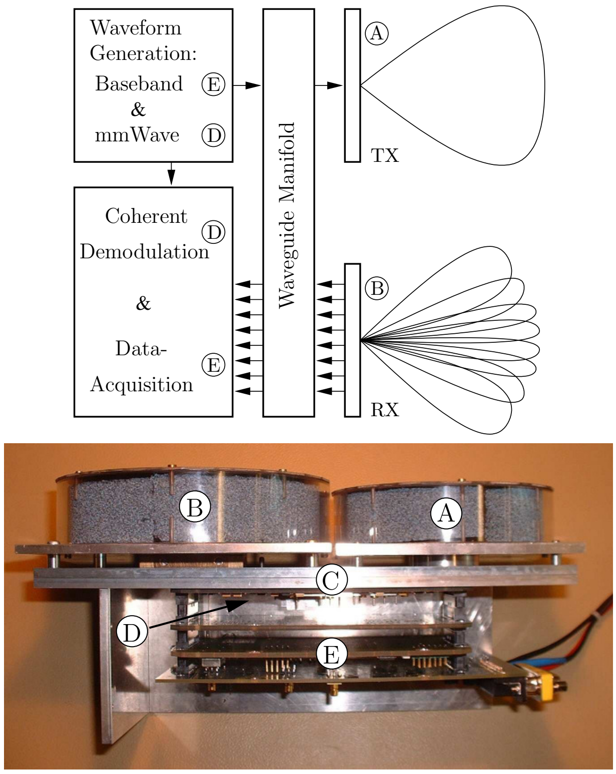

Fig. 1. Overview and photograph of the eight-channel FMCW radar sensor.

III. 2D-Radar Imaging

Based on the achieved antenna patterns a data model for the eight-channel FMCW radar sensor was developed. Considering the angle-continuous radar response only at N discrete points, the data model can be written in matrix form as

$$\vec{y} = \begin{bmatrix} p_1(\alpha_1) & p_1(\alpha_2) & \dots & p_1(\alpha_N) \\ p_2(\alpha_1) & p_2(\alpha_2) & \dots & p_2(\alpha_N) \\ \vdots & \vdots & \vdots & \vdots \\ p_8(\alpha_1) & p_8(\alpha_2) & \dots & p_8(\alpha_N) \end{bmatrix} \cdot \vec{x} = \mathbf{P} \cdot \vec{x} \quad (1)$$

The vector $\vec{x}$ contains the angle-discrete target response received from a certain range cell at N points. $\mathbf{P}$ is an $8 \times N$ matrix, which is derived from the antenna patterns of the

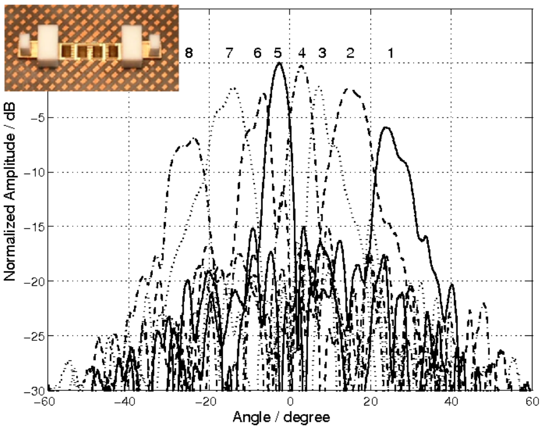

Fig. 2. Radiation patterns of the eight-channel RX antenna; dielectric feed elements are shown in the upper left corner.

TABLE I
DESCRIPTION OF THE STANDARD TARGET SCENARIO

Post number	Radial distance	Off-axis direction
1	13 m	$25°$
2	10 m	$-6°$
3	15 m	$-3°$

RX antenna. The multiplication of $\mathbf{P}$ and $\vec{x}$ leads to the eight element vector $\vec{y}$ providing the amplitude and phase information of the beat frequency signals.

Starting from this data model different 2D-imaging algorithms were developed, implemented, and verified using the described sensor setup and the radar system simulator presented in [5]. In both cases a standard target scenario consisting of 3 vertical metal posts is measured or serves as input for the simulation model respectively. The position of the posts is as in Table I and is chosen in a representative way. Post 1 is positioned at one main lobe direction of the RX antenna and post 2 at the intercept point of two adjacent RX antenna patterns. Post 3 is used to prove the wide angle coverage of the sensor.

A. *Monopulse principle*

A first approach to derive a two-dimensional radar image is to extend the classical monopulse principle to a two-dimensional imaging algorithm. This is done by considering the normalised difference pattern of two adjacent channels, which is defined as

$$S_{\Delta i} = \frac{S_i(\alpha) - S_{i+1}(\alpha)}{S_i(\alpha) + S_{i+1}(\alpha)}$$

where i is the number of one of the channels $1 \ldots 7$. Normalisation to the sum-pattern leads to an amplitude independent behaviour. Therefore this normalised difference pattern can serve as a "lookup-table" for determining the direction of a point target, which is unambiguous over a wide range between the two main lobe directions of channel i and $i+1$. Imaging can be done by calculating the normalised difference of the received signals y_{Δ_i} for each range cell

$$y_{\Delta i} = \frac{y_i - y_{i+1}}{y_i + y_{i+1}} = \frac{y_i - y_{i+1}}{y_{\Sigma i}}$$

and comparing this value to the normalised difference pattern using the following expression:

$$\hat{x}_i(\alpha) = \frac{y_{\Sigma i}}{|S_{\Delta i}(\alpha) - y_{\Delta i}| + \nu}$$

A value of $\nu \ll 1$ avoids a singularity of the expression at the actual target direction. Weighting with the sum signal $y_{\Sigma i}$ is necessary, because otherwise the algorithm were entirely amplitude independent, and also very small signals would lead to a significant response. To avoid ambiguities the expression is evaluated only *between* the main lobe directions of two adjacent channels.

Fig. 3 shows the result when applying the described monopulse imaging algorithm to measured data. The pseudocolor plot is normalised to the maximum value, and a brighter colour means a larger amplitude. It can be seen that the algorithm works best for targets positioned directly at the intercept point of the two antenna patterns (post 2). Targets which are picked up only by one antenna beam result into a slightly blurred but still significant response and can be detected properly (posts 1 and 3). The described monopulse imaging algorithm is non-linear and therefore not suitable in a multi-target environment or when objects cannot be approximated as single points. So a second method was developed based directly on the data model given before.

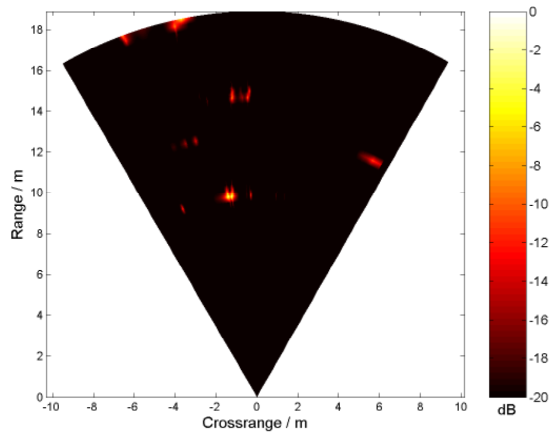

Fig. 3. Radar image of the standard target scenario obtained by applying the monopulse imaging algorithm to measured data.

B. *Complex-valued beamforming*

According to Equ. (1) the received vector $\vec{y}$ is always a linear combination of all possible reference vectors $\vec{p}_n$ namely the column vectors of $\mathbf{P}$. The idea is to compare the vector $\vec{y}$ with all vectors $\vec{p}_n$ simply by calculating the inner product. Thus an estimate $\hat{\vec{x}}$ of $\vec{x}$ can be given as

$$\hat{\vec{x}} = \mathbf{N} \cdot \mathbf{P}^H \cdot \vec{y} = \mathbf{N} \cdot \mathbf{P}^H \mathbf{P} \cdot \vec{x}\,.$$

The diagonal normalisation matrix $\mathbf{N}$ is introduced to compensate for angle dependent amplitude variations of the imaging procedure. Applying the method to a uniformly spaced linear antenna array shows that this approach is nothing else than a generalised formulation of beamsteering using the standard delay-and-sum approach.

The method of complex-valued beamforming was applied to data obtained by measurement, and the results are visualised using a pseudocolor plot (cf. Fig. 4). The presence and

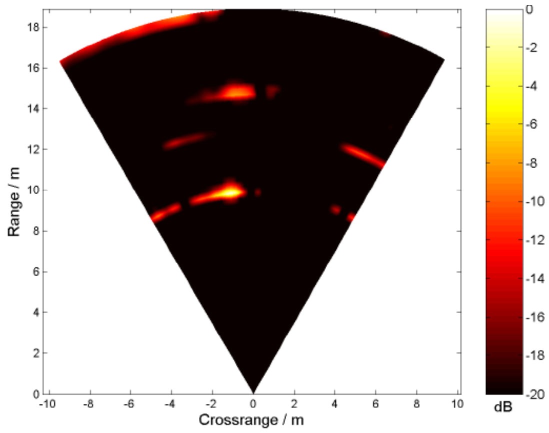

Fig. 4. Radar image of the standard target scenario obtained by applying the complex-valued beamforming algorithm to measured data.

the angular position of all targets can be detected with the expected accuracy. It should be mentioned that the angular resolution of all *linear* imaging techniques is limited due to the angular spacing of the antenna beams to the same degree as due to their beamwidths.

C. Beamforming applied to magnitude information

Complex-valued beamforming requires an exact knowledge of the phase relationship between the channels at each angle. Applying the same method only to the magnitude information avoids a complex calibration procedure. The underlying data model is slightly modified to

$$\vec{y}_a = \text{abs}(\mathbf{P}) \cdot \text{abs}(\vec{x}) = \mathbf{P}_a \cdot \vec{x}_a \, .$$

This is quite similar to the model used before, but applying the same imaging method results into a relatively high sidelobe level. This is caused by the fact that all components of the receive- and reference-vectors are positive and unequal to zero. Therefore, the mutual inner product is positive at all angles as well. To overcome this, a transformation matrix $\mathbf{T}$ can be found which transforms 8 properly chosen reference vectors $\vec{p}_{a,i}$ into an orthogonal basis. Normally, the reference vectors corresponding to the antennas' main lobe directions should be used. Applying this transformation to the vector $\vec{y}$ and all reference vectors $\vec{p}_{a,n}$ assures that a target at one main lobe direction leads to a zero response at any other mainlobe direction. With $\mathbf{P}_a = \text{abs}(\mathbf{P})$ and $\vec{y}_a = \text{abs}(\vec{y})$ the imaging algorithm reads

$$\hat{\vec{x}} = \mathbf{N} \cdot (\mathbf{T} \cdot \mathbf{P}_a)^T \cdot \mathbf{T} \cdot \vec{y}_a \, .$$

Fig. 5 shows what happens to 8 exemplary antenna patterns due to the described coordinate transformation. It can be

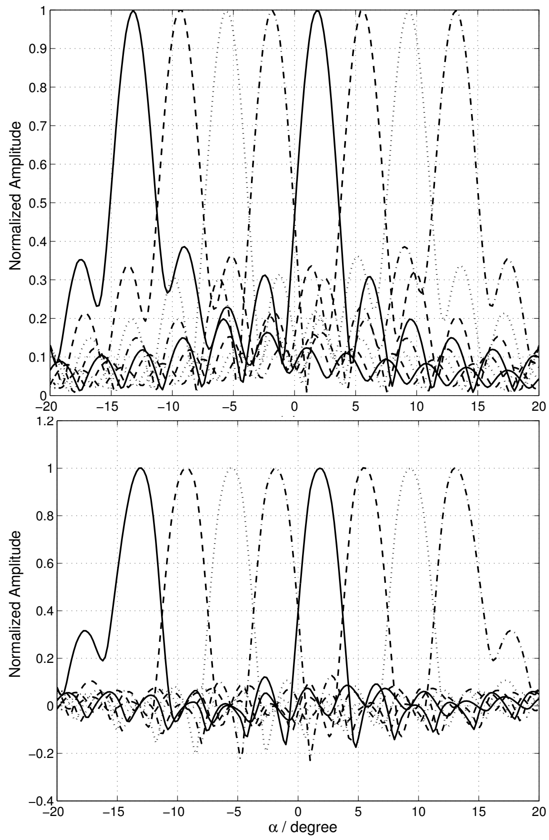

Fig. 5. Exemplary antenna patterns before and after coordinate transformation.

clearly seen that at the mainlobe direction of one channel the amplitude of all other channels is forced to zero. In other words, the reference vectors in the data model are orthogonal at these angular positions, and their mutual inner product is zero. Additionally, the transformed antenna patterns have a significantly lower sidelobe level compared to the original patterns which is the main requirement for achieving a flat response of the imaging algorithm.

The measurement results are shown in Fig. 6. With the reduced complexity in mind, this method of partially orthogonalising the antenna patterns shows a good performance even compared to complex-valued beamforming.

For completeness it should be said that there are other techniques to improve resolution by means of linear operations. And of course all of them can be applied to complex-valued data as well. The most common approach of solving an underdetermined problem like Equ. (1) is the so called pseudo-inverse matrix.

D. MUSIC algorithm

In [6] a parameter estimation algorithm called MUSIC (MUltiple SIgnal Classification) is described. The MUSIC algorithm belongs to the group of so-called signal subspace methods. These methods are intended to identify a finite

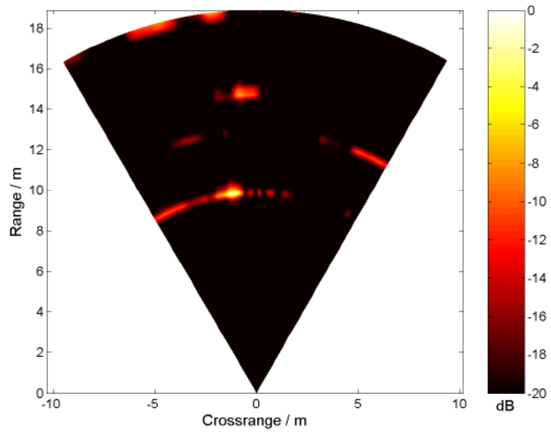

Fig. 6. Radar image of the standard target scenario obtained by applying the magnitude beamforming algorithm to measured data.

number of sinusoidal signals in a multidimensional signal space.

In [6] MUSIC is presented as an one-dimensional direction of arrival (DOA) estimator. To extend this algorithm to the second (range) direction the data model has to be frequency-dependent. This can be achieved by considering a virtual second sensor array, which is generated by simply delaying the time domain signals by a certain amount of time τ (e.g. one sampling period). Thus the data model reads

$$\mathbf{P}_{\text{MUSIC}} = \left[\begin{array}{c} \mathbf{P} \\ \mathbf{P} \cdot \mathrm{e}^{-\mathrm{j} \cdot \omega \cdot \tau} \end{array} \right] .$$

The dimension of the signal space is increased by a factor of 2. Compared two [6] the MUSIC pseudo-spectrum has to be evaluated for each pair of range and cross-range values, which requires a very high computational effort. To decrease the complexity, a first guess of the targets could be gathered from one of the other beamforming methods. In this case the calculation of the MUSIC pseudo-spectrum could be restricted to some small areas.

The simulation results show a very good resolution in both dimensions (cf. Fig. 7). The application on measured data suffers from the problem that the MUSIC algorithm expects the signals induced by one target to appear *coherent* at all channels. Otherwise, all off-diagonal elements of the covariance matrix would converge to zero for a long observation time, and the eigenvalue decomposition would not lead to the correct solution. Considering the different path lengths introduced e.g. by the waveguide manifold the restriction of coherency cannot be preserved because of the slightly different intermediate frequencies. Additionally, MUSIC depends on the exact knowledge of the data model more than all other methods described before. Probably these problems can be overcome by some calibration procedures, which will be the topic of further investigations.

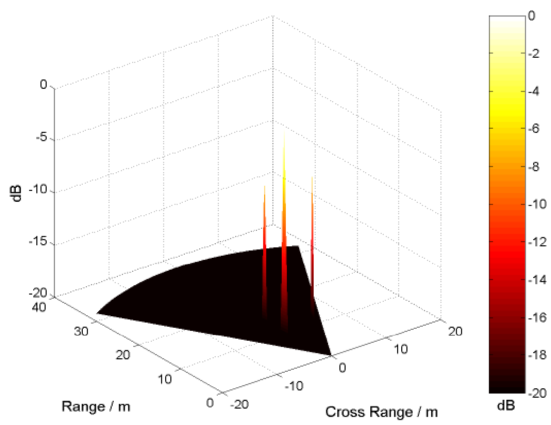

Fig. 7. Result of the 2-dimensional MUSIC algorithm applied to simulated data.

IV. Comparison

All described radar imaging algorithms can be subdivided into linear (complex-valued and magnitude beamforming) and non-linear (monopulse and MUSIC) methods. Non-linear processing can provide a high angular resolution in scenarios with a smaller number of objects per range cell while linear processing is well suited in multi-target environments.

Another advantage of all linear techniques is that they are based on the multiplication of matrices which can be precomputed and stored in a non volatile memory. That means that the computation itself can be reduced to simple multiply-and-accumulate (MAC) operations and is therefore predestined for implementation on a standard digital signal processor (DSP).

V. Conclusion

Different cross-range resolution techniques for a multi-channel FMCW sensor were described. They have been implemented and verified by means of simulation and tested using an eight-channel experimental sensor.

Even though the main focus of this work was on imaging it could be shown that the proposed algorithms provide a sufficient resolution to detect and distinguish a certain number of objects over a wide angular range. Therefore the generated data are suited to serve as input for additional units implementing the object tracking and classification functionality needed for the next generation ACC systems.

References

[1] C. Metz, E. Lissel, and A. F. Jacob, “Planar multiresolutional antenna for automotive radar,” *European Microwave Conference*, 2001.

[2] W. Mayer, M. Meilchen, W. Grabherr, P. Nüchter, and R. Gühl, “Eight-channel 77 GHz front-end module with high-performance synthesized signal generator for FMCW sensor applications,” *IEEE Transactions on Microwave Theory and Techniques*, vol. 52, No. 3, pp. 993–1000, March 2004.

[3] R. Leberer and W. Menzel, “Shaped-beam reflectarrays,” *Asia Pacific Microwave Conference*, 2004.

[4] W. Menzel, M. Al-Tikriti, and R. Leberer, “A 76 GHz multiple-beam planar reflector antenna,” *European Microwave Conference*, vol. 3, pp. 977–980, 2002.

[5] W. Mayer and W. Menzel, “On the effects of non-ideal signal sources in automotive short range FMCW sensors,” *International Radar Symposium*, pp. 141–145, 2005.

[6] R. O. Schmidt, “Multiple emitter location and signal parameter estimation,” *IEEE Transactions on Antennas and Propagation*, vol. AP-34, No. 3, March 1986.